GEOSCIENCE FRONTIERS 3(5) (2012) 587–602

available at www.sciencedirect.com

China University of Geosciences (Beijing)

GEOSCIENCE FRONTIERS

journal homepage: www.elsevier.com/locate/gsf

GSF FOCUS

The Tuerkubantao ophiolite mélange in Xinjiang, NW China: New evidence for the Erqis suture zone

Yuwang Wang [a,b,c,d,*], Jingbin Wang [a,b,c,d], Lijuan Wang [a,b,c], Lingli Long [a,c], Pingzhi Tang [a,c], Zhen Liao [a,c], Huiqiong Zhang [a,c], Yu Shi [d]

[a] *Beijing Institute of Geology for Mineral Resources, Beijing 100012, China*
[b] *Key Laboratory of Mineral Resources, Institute of Geology and Geophysics, CAS, Beijing 100029, China*
[c] *Sino Tech Metals Exploration Co., Ltd., Beijing 100012, China*
[d] *China University of Geosciences (Beijing), Beijing 100083, China*

Received 9 December 2011; received in revised form 6 February 2012; accepted 7 February 2012
Available online 17 February 2012

KEYWORDS
Ultramafic-mafic rocks;
Geochemistry;
U-Pb zircon geochronology;
Tectonics;
Subduction;
Collision

Abstract The extension of the suture zone between the Siberian and Kazakhstan continents in China has been a matter of debate because few outcrops of ophiolitic mélange have been found so far. The recently found Tuerkubantao ophiolitic mélange, which is located east of the Kekesentao Mt. in the Buerjin County of the Chinese Altay, provides an important clue for this problem. This paper presents the results of field investigation, petrology, U-Pb isotope dating of zircons and bulk-rock geochemistry of the Tuerkubantao mélange rocks. The mélange consists of fault-contacted ultramafic rocks, gabbro, diabase, basalt, flysch and granitoids. The ultramafic-mafic rocks are Mg-rich ($^{\#}Mg = 4.25–6.35$) and $w(SiO_2)$ spans 38.8%–46.8%. Basalt and gabbro are geochemically similar and are characterized by low $w(FeO_t)$ (10.9%), total alkali $w(Na_2O + K_2O) = 2.58\%$) and $w(TiO_2)$ (1.17%) and affinity to the Mg-rich tholeiite series. The flat REE and trace-element patterns of the ultramafic-mafic rocks are indicative of their ophiolite origin, i.e., formation in a mid-oceanic ridge setting. The fragments of low-K gneissic granite formed in suprasubduction or syn-collisional setting. Zircons from gabbro and gneissic granite yielded U-Pb ages of 363 and 355 Ma, respectively, suggesting Late Devonian mid-oceanic

* Corresponding author. Tel.: +86 10 84921365; fax: +86 10 8492223.
E-mail address: wyw@cnncm.com (Y. Wang).

Peer-review under responsibility of China University of Geosciences (Beijing).
doi:10.1016/j.gsf.2012.02.002

spreading and oceanic subduction accompanied by suprasubduction magmatism. The Tuerkubantao ophiolite together with the Qiaoxiahala and Buergen ophiolites of the Kekesentao belt define an ophiolitic mélange belt extending along the Erqis fault. This belt probably belongs to the Ural-Zaisan-South Mongolian suture-shear zone formed during the subduction of the Paleo-Asian Ocean and subsequent collision of the Siberian and Kazakhstan continents.

1. Introduction

It is generally accepted that the Central Asian Orogenic Belt (CAOB), the world's largest accretionary orogen, was largely formed by subduction of the Paleo-Asian Ocean and accretion of oceanic seamounts and plateaus, ophiolites and collision of ancient microcontinents, arc terranes and successions of passive continental margins (Sengör et al., 1993; Yin and Nie, 1996; Jahn et al., 2004; Safonova et al., 2004, 2011; Xiao et al., 2004, 2009). The CAOB includes the Ural-Zaisan-South Mongolian zone, which is a suture of the Paleo-Asian Ocean (PAO), which once separated the Altai-Mongolian and Kazakhstan-Junggar terranes (Xiao et al., 1992, 2004, 2009; He and Li, 2000; Buslov et al., 2001, 2004; Badarch et al., 2002; Yakubchuk, 2004; Li et al., 2006a; Wu et al., 2006; Rippington et al., 2008; Glorie et al., 2011; Pirajno et al., 2011; Long et al., 2012). Remnants of paleo-oceans are preserved in ophiolitic belts and ophiolitic mélanges, the study of which is necessary for unraveling their evolution in the context of global plate tectonics (Coleman, 1977; Pearce et al., 1984; Stern et al., 1989; Bloomer et al., 1989; Gribble et al., 1996; Safonova et al., 2009; Dharma Rao et al., 2011). However, fragments of paleo-ophiolites are usually sparse and discontinuous in the Ural-Zaisan-South Mongolian zone. It is still unclear where is the suture boundary between the Siberian and Kazakhstan continental blocks in China, how far the ophiolitic belt extends and how it is linked with other ophiolite occurrences of the CAOB. For example, according to Zonenshain et al. (1990) and Yakubchuk (2004) the Zaisan ophiolitic mélange in East Kazakhstan has no continuation in China. However, the southern Altaids host numerous ophiolite slivers, which are interpreted by many Chinese geologists as fragments of the Siberia-Kazakhstan suture, which extends into China and includes: (1) the Erqis fault (Ren et al., 1980), (2) the Kelamali ophiolite belt (Li et al., 1982; Ma et al., 1997), (3) the Aermantai-Zhaheba-Kekesentao ophiolite belt (He et al., 1990, 1994), and (4) the Kekesentao ophiolitic mélange belt (Wang et al., 1999).

The Erqis fault has been previously considered as a strike-slip zone with a thick mylonite zone (Sengör et al., 1993), and as a narrow sliver containing 10–15 km-wide mylonite zones, which has undergone a sinistral displacement to a distance of at least 1000 km (Sengör et al., 1993; Laurent-Charvet et al., 2003; Buslov et al., 2004). In northern Xinjiang the Erqis fault is named Erqis-Buergen tectonic zone and many researchers regarded it a suture-shear zone as well (Ren et al., 1980; Wang et al., 1999). However, it is hard to identify this suture conclusively because there are few outcrops of "ophiolitic mélange". Although many geologists have speculated about an ophiolitic belt along the Erqis tectonic zone (Zhang, 1981; Liu, 1983; Cao, 1994; He et al., 1994; Chen et al., 1997; Niu et al., 1999, 2006; Yu et al., 2000; Zhang and Zhou, 2001; Wang et al., 2003; Xu et al., 2003; Zhang et al., 2003b, 2008b; Li et al., 2006a; Xiao et al., 2009), ophiolite complexes have been so far confirmed only in the Qiaoxiahala and Buergen localities, east of the Erqis zone (Wu et al., 2006). The Kekesentao "quasi-ophiolite", which is located west of the zone, has been reported before many times (Zhang, 1981; Cao, 1994; He et al., 1994; Zhang et al., 1996; Xu et al., 2001; Wang et al., 2003; Niu et al., 2006; Wang and Xu, 2006; Xiao et al., 2009; Dong et al., 2010), but the previous researches mentioned ultramafic rocks only without gabbro, submarine basalt and deep-sea sediments. Therefore, its detailed study seems to be necessary.

During the recent field studies of the Kekesentao mountains area located southwest of Buerjin town, North Xinjiang, we discovered a set of ultramafics, gabbro, diabase, basalt and flysch formations in the Tuerkubantao district. We studied this section and recognized it as a fragment of ophiolitic mélange. This paper presents U-Pb zircon ages and petrologic and geochemical data on Tuerkubantao mélange-hosted ultramafic rocks, gabbro, basalt, diorite and granite.

2. Regional geology and rock lithology

The newly discovered Tuerkubantao ophiolitic mélange is located east of the Kekesentao Mountain and is a part of the Kekesentao ophiolite belt (Fig. 1). The available outcrops in the Kekesentao area are dominated by the Middle Devonian Yundukala Formation (D_2y). According to a Regional Survey Report (1/200,000) of the Geological Bureau of Xinjiang Uygur Autonomous Region (1983), this formation can be divided into two sub-formations. Lithologically, the lower sub-formation (D_2y^a) is sandy slate intercalated with siliceous rocks and tuffaceous siltstone and the upper sub-formation (D_2y^b) is sandy slate intercalated with quartzite, limestone, etc. In addition, in the south, there are outcrops of mudstones, siltstones and limestones of the Lower Carboniferous Nalinkala Formation (C_1n), as well as calcareous sandstones and mudstones of the Upper Carboniferous Qiaqihai Formation (C_2q). A Hercynian granitic batholith outcrops in the northern part of the Kekesentao area over approximately 140 km^2 and intrudes the Yundukala Formation (D_2y). The batholith is dominated by porphyritic biotite granite with subordinate red feldspar giant-grained granite, gray biotite granite, and biotite quartz diorite. There are also intrusions of Hercynian granitic porphyry including haplophyre (porphyroclastic granite), biotite granite porphyry, hornblende granite porphyry, plagioclase granite porphyry, granodiorite porphyry, etc., generally as apophyses or dykes occupying an area of less than 10 km^2. East of the Kekesentao area, near Tuerkubantao, there are outcrops of gneissic granite and biotite oligoclase granite (Fig. 1).

The Tuerkubantao ophiolitic mélange is located east of the Kekesentao area and includes fragments of ultramafic rocks, gabbro, diabase, basalt, siliceous rocks, and a flysch formation. The WNW-ESE striking mélange zone is up to 4 km wide (Fig. 2).

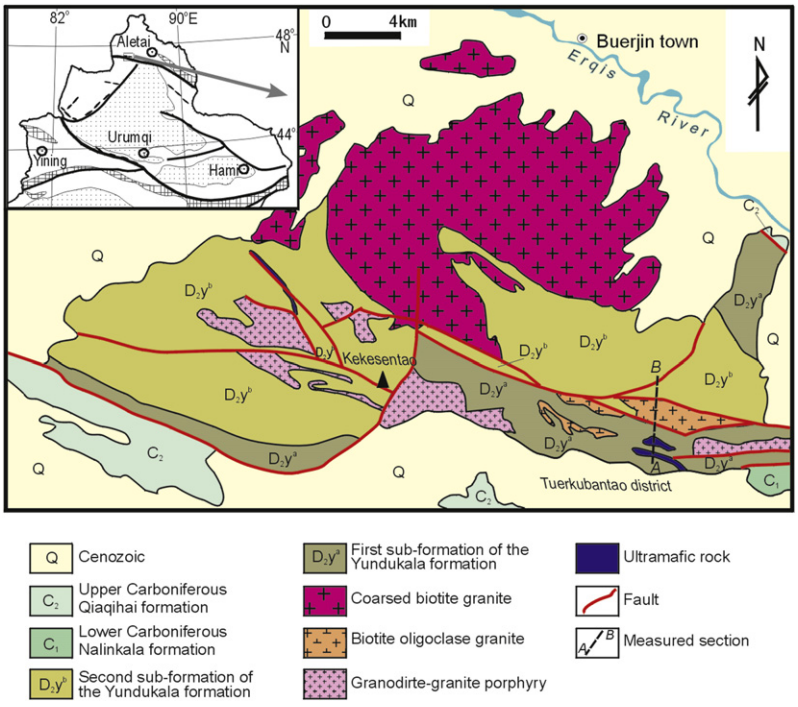

Figure 1 Sketch geological map of the Kekesentao area.

The section includes (from south to north) gabbro, three ultramafics zones, xenolith-bearing gneissic granite, xenolith-bearing flysch formation intercalated with basalt. The Middle Devonian Series of argillite and sandstone (D_2y) outcrops in the northernmost part of the section. The rock units are separated by faults and zones of shearing and mylonitization, which range in thickness from 10 cm to approximately 2 m.

The layers of ultramafic rocks are about 6 km long and 20–500 m wide (Fig. 3A). The rocks have been metamorphosed and strongly serpentinized and have clear tectonic contacts with adjacent rocks (Fig. 3B). Gabbro bodies occur in the southern part of the section (Fig. 2) interspaced with ultramafic rocks. They have undergone low-grade metamorphism and cut by diabase and granitic dykes/veins and contain xenoliths of light-colored rocks (e.g., plagioclase granite). Basalts occur as lava flows and have undergone post-magmatic alteration. Gneissic granite usually contains abundant xenoliths of felsic schist, plagioclase-hornblende schist, hornfels, siliceous rocks, gabbro and granodiorite (Fig. 3C), which, according to the lithology of surrounding geologic units, could have been derived from the northern Devonian formation and/or southern ophiolite suite. The flysch formation is dominated by rhythm-like sandy and argillaceous rocks interlayered with thin-bedded siliceous rocks, chlorite schist, basalt and mafic tuff (Fig. 3D), which also contain numerous xenoliths of altered and

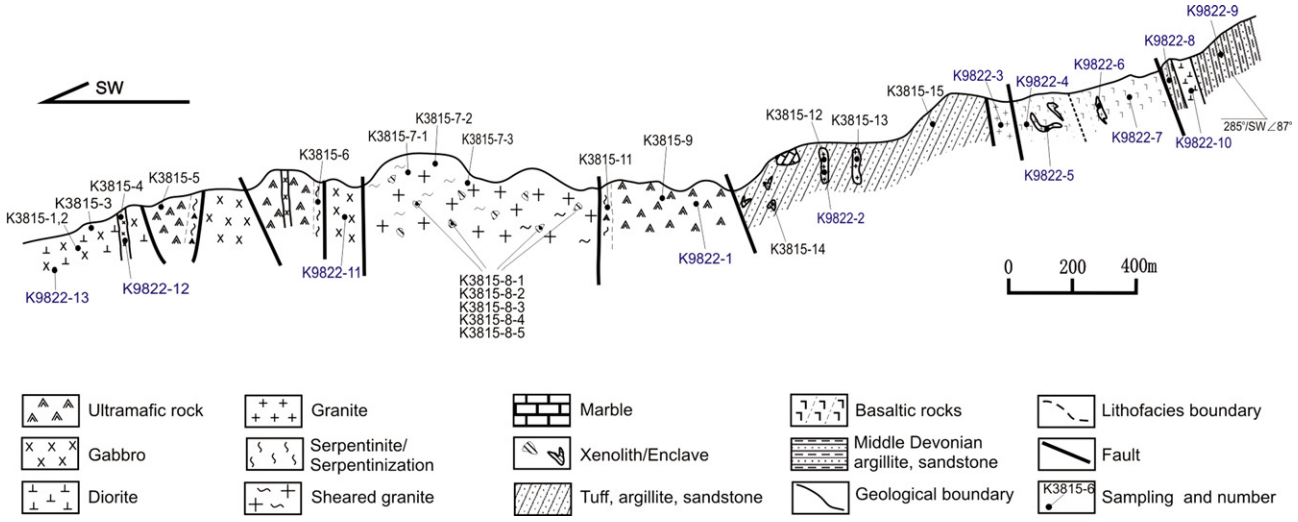

Figure 2 Geological section of the Tuerkubantao ophiolitic mélange.

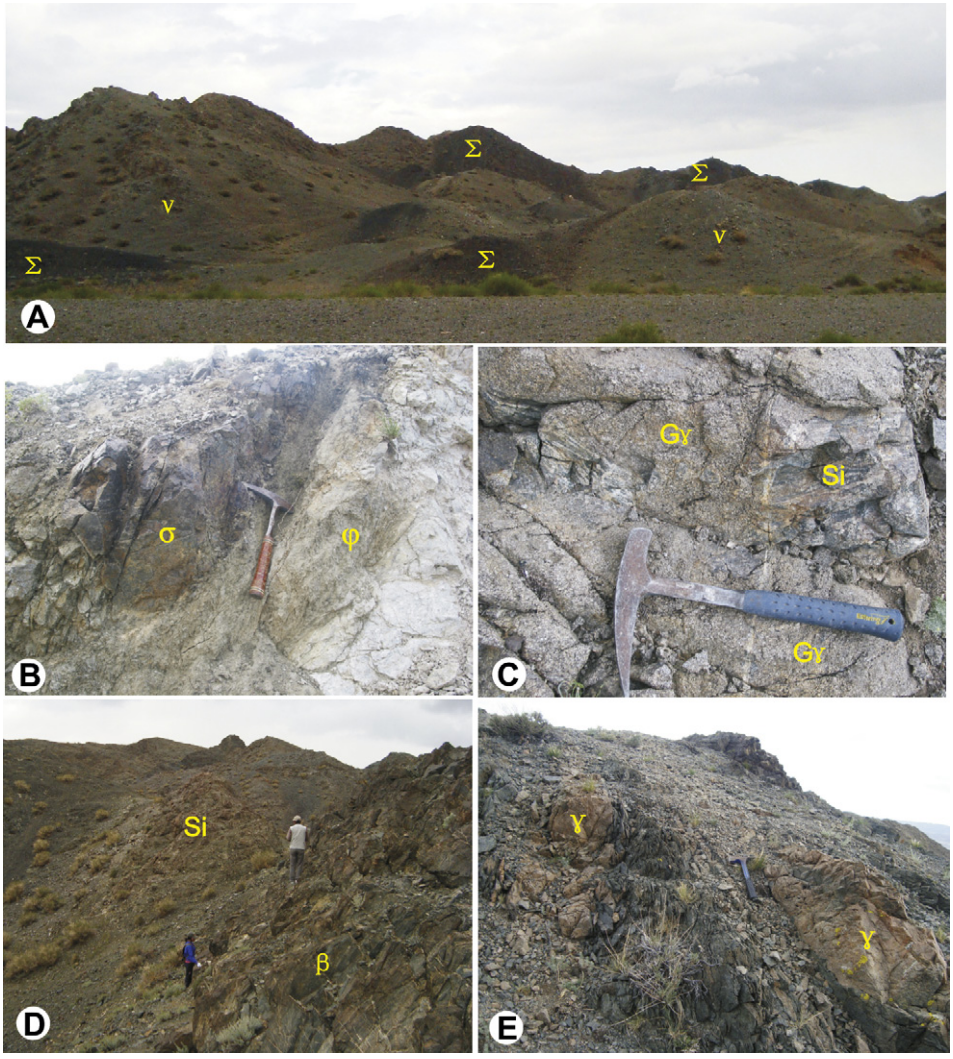

Figure 3 Field photographs of the Tuerkubantao ophiolitic mélange.
A: mélange belt of ultramafic rock (Σ) and gabbro (ν); B: serpentinite (φ) band in the margin of peridotite (σ); C: gneissic granite (Gγ) containing siliceous rocks (Si) and granulite xenoliths; D: siliceous rocks (Si) and basalt (β) interbed in flysch formation; E: broken granite (γ) in flysch formation.

deformed granodiorite and granite (Fig. 3E). The formation contains no chert and carbonate. Like other rock units of the ophiolitic mélange, the flysch formation shows fault contacts with ultramafic rocks.

3. Petrology

The ultramafic rocks of the study area are mainly lherzolite and peridotite possessing poikilitic texture (Fig. 4A). The mineral assemblages are dominated by olivine and clinopyroxene with subordinate hornblende and orthopyroxene and accessory picotite (Fe-Cr spinel), magnetite and sulfide. Gabbro is medium to coarse grained with pyroxene poikilitic texture (Fig. 4B) and consists of labradorite, augite and less abundant hornblende and magnetite. Diorite and granodiorite are medium to coarse granular (Fig. 4C), with dominate hornblende, oligoclase to andesine plagioclase, subordinate biotite and quartz and accessory sphene, apatite and magnetite. Macroscopically, the xenoliths of fine-grained granitoids look fresh, red, gray or creamy white. Microscopically, they possess porphyroid structure (Fig. 4D) and contain quartz (20%–35%), plagioclase (20%–50%), potassium feldspar (10%–50%), subordinate biotite, and accessory apatite and zircon. Gneissic granite is grayish white and possesses medium to fine-grained structure (Fig. 4E); its mineral assemblage consists of dominant oligoclase, microcline (often as perthite intergrowths), and quartz, subordinate biotite and accessory apatite, zircon, tourmaline, and garnet. Gray and green massive or sheared basalts are dominated by clinopyroxene, which is almost completely replaced by light-colored hornblende, and sericitized plagioclase (Fig. 4F).

4. Methods

We have systematically collected samples of various rocks of the ophiolitic mélange (Figs. 2 and 3). Based on careful microscopically study, we selected several representative samples for geochemical analysis (major and trace elements). The major elements were analyzed by a XRF-1500 X-ray fluorescence spectrometer in the Key Laboratory of Mineral Resources of the

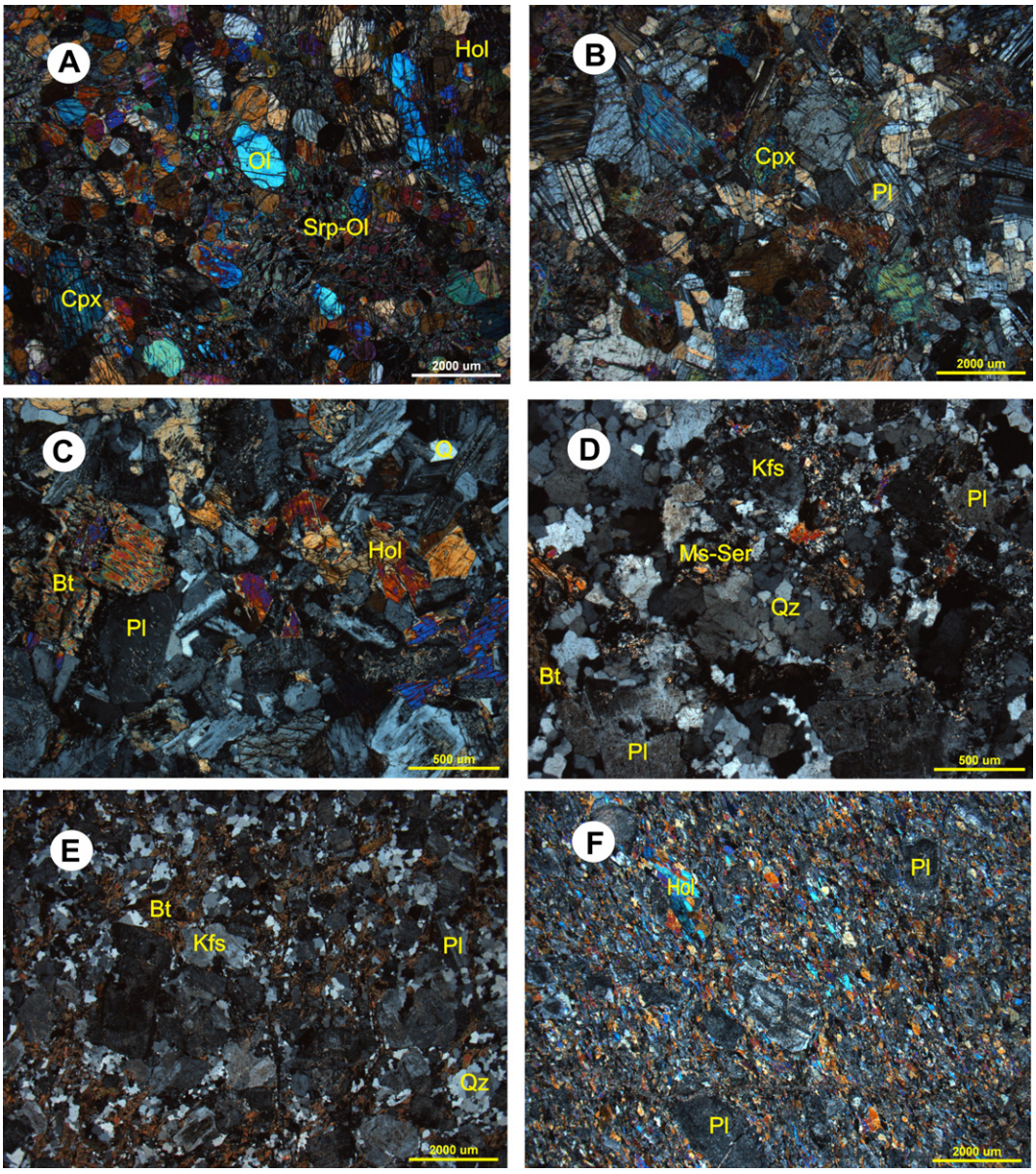

Figure 4 Photomicrographs of the Tuerkubantao ophiolite.
A: pyrolite (K9822-1); B: gabbro (K9822-12); C: diorite (K9822-11); D: granite (K9822-6); E: gneissic granite (K3815-7-2); F: basalt (K9822-7). Mineral index: Ol – olivine; Srp – serpentine; Cpx – clinopyroxene; Hol – hornblende; Bt – biotite; Pl – plagioclase; Kfs – potassium feldspar; Qz – quartz; Ms – muscovite; Ser – sericite.

Institute of Geology and Geophysics, Chinese Academy of Sciences and by a Philips PW2404 X-ray fluorescence spectrometer in the Analytical Laboratory of CNNC Beijing Research Institute of Uranium Geology. The slice melting method was applied for determining concentrations of SiO_2, TiO_2, Al_2O_3, Fe_2O_{3t}, MnO, MgO, CaO, Na_2O, K_2O and P_2O_5, the potentiometry method – for CO_2, the weight method – for H_2O^+ and H_2O^- and the volumetric method – for FeO. Rare earths and trace elements were analyzed by inductively coupled plasma mass spectrometry (ICP-MS) using the "In" internal standard solution on an "ELEMENT" analyzer in the ICP-MS Laboratory of the Institute of Geology and Geophysics, Chinese Academy of Sciences. For quality control the standard and parallel samples were analyzed during all analytical runs. The data were carefully verified and, if necessary, corrected to achieve their high accuracy. The analytical results are shown in Table 1. The details of U-Pb zircon dating analytical procedure are presented in Section 6.

5. Geochemistry

5.1. Major elements

The concentrations of SiO_2, Al_2O_3, FeO_t·(FeO + 0.899*Fe_2O_3), MgO and CaO in Tuerkubantao peridoties and lherzolites are close to the average values of these major oxides in ophiolite-type ultramafic rocks of China, which were calculated by Dong et al. (1995). In contrast, the concentrations of other major oxides,

Table 1 Major (%) and trace (ppm) elements in rocks of the Tuerkubantao ophiolitic mélange.

Rocks	Basalt	Mafic-ultramafic rocks			Gabbro		Diorite	Granodiorite	Gneissic granite		Granitoid xenolith			Diorite xenolith
Samp. Nos.	K9822-7	K3815-5	K3815-10	K9822-1	K3815-3	K9822-12	K9822-11	K9822-3	K3815-7-2	K3815-7-3	K9822-6	K3815-12	K3815-13	K3815-8-5
SiO_2	49.34	38.84	46.84	38.90	52.64	45.05	55.52	69.58	66.36	68.5	77.04	74.6	75.48	55.42
TiO_2	1.17	0.10	0.18	0.20	0.24	0.14	0.49	0.39	0.7	0.67	0.13	0.1	0.22	0.59
Al_2O_3	13.11	6.71	2.6	1.62	16.03	18.27	14.23	13.77	14.19	12.37	11.28	12.12	12.43	15.89
Fe_2O_3	3.53	5.41	3.43	9.24	0.94	0.74	2.75	1.10	1.34	1.57	0.26	0.52	1.18	1.36
FeO	7.70	4.65	5.32	5.40	6.32	2.25	6.20	2.10	3.98	3.62	0.45	0.53	1.03	5.36
MnO	0.20	0.12	0.19	0.30	0.143	0.08	0.27	0.08	0.17	0.18	0.01	0.04	0.05	0.21
MgO	8.02	30.83	30.66	33.46	8.71	10.28	7.35	1.46	3.61	3.18	0.29	0.34	0.69	6.68
CaO	10.49	2.89	5.18	3.18	8.53	16.82	6.18	1.71	2.49	4.59	2.85	1.4	0.8	7.1
Na_2O	2.07	0.27	0.26	0.26	3.18	0.67	2.71	4.08	2.74	1.91	6.04	2.49	4.13	1.96
K_2O	0.51	0.04	0.06	0.05	0.66	0.58	0.91	3.15	1.76	1.26	0.21	6.3	2.81	2.5
P_2O_5	0.12	0.02	0.02	0.02	0.02	0.01	0.13	0.08	0.1	0.15	0.04	0.05	0.03	0.07
LOS	2.64	9.31	4.84	6.63	2.06	4.31	2.32	2.10	2.28	1.7	1.24	1.28	1.1	2.17
$\sum$	98.90	99.19	99.58	99.26	99.47	99.20	99.06	99.59	99.72	99.70	99.85	99.77	99.96	99.31
$Na_2O + K_2O$	2.58	0.31	0.32	0.31	3.84	1.25	3.62	7.23	4.50	3.17	6.25	8.79	6.94	4.46
K_2O/Na_2O	0.25	0.15	0.23	0.20	0.21	0.87	0.34	0.77	0.64	0.66	0.03	2.53	0.68	1.28
M/F[a]	1.29	5.70	6.35	4.25	2.12	6.11	1.46	0.82	1.20	1.09	0.74	0.59	0.57	1.75
La	4.17	0.23	0.43	0.49	1.11	1.21	11.2	16.0	24.1	20.8	10.20	8.80	17.4	7.80
Ce	10.0	0.61	1.32	1.35	2.87	2.79	23.4	35.3	52.0	42.6	22.3	17.2	35.1	17.9
Pr	1.52	0.09	0.21	0.20	0.46	0.36	2.60	3.85	6.04	5.14	2.61	2.12	4.00	2.30
Nd	8.21	0.43	1.14	1.04	2.43	1.93	10.4	15.5	23.2	19.3	10.4	8.07	14.1	9.52
Sm	2.63	0.14	0.40	0.39	0.90	0.51	2.21	3.43	5.08	4.38	2.80	2.05	3.04	2.80
Eu	0.93	0.08	0.13	0.13	0.48	0.40	1.10	0.76	1.00	1.15	0.33	0.56	0.53	0.90
Gd	3.02	0.18	0.49	0.41	1.15	0.62	2.08	3.58	4.33	3.89	2.83	2.27	2.81	2.98
Tb	0.72	0.04	0.10	0.10	0.24	0.13	0.41	0.74	0.68	0.62	0.71	0.47	0.48	0.57
Dy	4.81	0.24	0.66	0.67	1.65	0.85	2.59	4.99	3.81	3.66	4.54	3.27	2.93	3.70
Ho	1.05	0.06	0.15	0.15	0.37	0.18	0.51	1.02	0.77	0.76	0.90	0.74	0.66	0.81
Er	3.30	0.17	0.43	0.46	1.02	0.58	1.58	3.09	2.11	2.13	3.00	2.16	1.97	2.36
Tm	0.56	0.03	0.07	0.08	0.16	0.09	0.27	0.56	0.32	0.33	0.57	0.36	0.33	0.37
Yb	3.43	0.18	0.42	0.47	1.03	0.64	1.89	3.30	2.15	2.21	3.66	2.38	2.25	2.53
Lu	0.56	0.03	0.07	0.08	0.16	0.10	0.29	0.55	0.33	0.34	0.62	0.36	0.37	0.38
Y	28.2	2.46	4.38	3.64	9.78	5.26	14.6	29.0	20.3	20.0	27.9	19.7	17.5	20.6
Rb	22.4	0.92	1.18	1.72	19.9	14.9	28.3	88.3	58.5	42.2	7.56	91.2	54.0	93.3
Sr	148	18.6	27.6	14.8	242	376	224	188	192	214	70.5	119	109	196
Ba	35.0	1.70	3.64	6.49	84.7	131	107	370	256	157	26.1	944	385	288
Nb	4.96	1.01	1.03	0.16	1.90	0.14	3.77	11.5	10.4	9.44	10.9	2.61	6.09	4.47
Ta	0.36	0.04	0.04	0.03	0.11	0.02	0.32	0.85	0.72	0.64	2.35	0.36	0.72	0.31
Zr	43.5	8.00	9.27	6.35	10.3	6.64	27.4	171	177	179	114	51.0	115	82.6
Hf	1.44	0.18	0.26	0.23	0.29	0.24	1.02	4.69	5.07	5.06	4.28	1.94	4.15	2.41

Th	0.423	0.11	0.12	0.14	0.27	0.15	3.66	7.30	8.53	4.81	7.68	7.65	10.2	2.50
U	0.15	0.04	0.05	0.05	0.22	0.04	0.86	1.13	1.07	1.12	1.63	0.86	1.41	0.52
Cr	207.0	2209	2523	1254	138	396	254	16.1	87.7	136	4.46	9.36	8.23	157
ΣREE	44.91	2.49	6.00	6.03	14.03	10.38	60.53	92.66	125.88	107.36	65.48	50.79	85.93	54.90
ΣLR/HR	1.57	1.72	1.53	1.49	1.43	2.27	5.29	4.20	7.69	6.70	2.89	3.23	6.29	3.01
δEu	1.01	1.57	0.88	1.02	1.45	2.18	1.55	0.65	0.64	0.84	0.36	0.79	0.54	0.95

[a] M/F = MgO/(FeO + 2*Fe_2O_3 + MnO) where oxides are in moles (%).

such as TiO_2, K_2O and P_2O_5, are relatively low. The Tuerkubantao ultramafic rocks are characterized by M/F values ranging from 4.25 to 6.35 (Table 1) and MgO content lower than the average (43.58%) of the metamorphic peridotite in China, but close to the average value of 492 ultramafic complexes (31.54%) or a little bit higher than that. On the whole, the major element composition of Tuerkubantao ultramafic rocks is similar to that of typical ophiolites. Gabbro is characterized by low Al_2O_3, alkali ($Na_2O + K_2O$) (Fig. 5a) and TiO_2 contents. The σ value (Rittmann Index) is between 0.76 and 1.53. The low contents of FeO_t and relatively high MgO results in high M/F value, which range from 2.12 to 6.11, match the composition of ophiolite-type gabbro. The chemical composition of basalt is similar to that of gabbro, featuring low FeO_t, $Na_2O + K_2O$ contents and TiO_2 and high MgO. In general, the basalts possess chemical affinities of the high Mg tholeiite series. Diorite, granodiorite and gneissic granite or granodiorite (Fig. 5a) are characterized by low alkali and high FeO_t and MgO contents. The ratio of K_2O/Na_2O is less 1 suggesting that these rocks belong to the sodium rock series.

Compositionally, the granitoid xenoliths are similar to the standard alkali granite (Wang and Zhou, 1982) with relatively low Al_2O_3, high ($Na_2O + K_2O$) and medium alkalinity, σ value varies between 1.15 and 2.45. The ratio of K_2O/Na_2O is variable and can be both less and more than 1. The chemical compositions of the diorite xenoliths are similar to the average compositions of worldwide diorites (Wang and Zhou, 1982), but have lower SiO_2 and Na_2O contents and higher MgO and K_2O contents. Accordingly we regard them as high-potassium basic diorite.

Thus, the above lithological types, i.e., peridotite, gabbro and basalt, are enriched in MgO, which is consistent with their suggested ophiolitic origin. The chemical compositions of gabbro, diorite, granodiorite and gneissic granodiorite are transitional in the SiO_2-K_2O diagram: all samples plot on the line separating the low-potassium (tholeiitic) and medium-potassium (calc-alkaline) series (Fig. 5b). The xenoliths of granitoids (granite and diorite) are enriched in alkali, especially in potassium resulting in $K_2O/Na_2O > 1$.

5.2. Trace elements

The concentrations of the REE in mafic-ultramafic rocks are relatively low: ΣREE is commonly lower than 50 ppm, less than 10 ppm in peridotite, 10–15 ppm in gabbro, and 44.91 ppm in basalt. The LREE and HREE are relatively low fractionated (Fig. 6a): the ratios of ΣLREE/ΣHREE range from 1 to 2, $(Gd/Yb)_n \leq 1$, $(La/Sm)_n \leq 1$. The gabbro and several peridotite samples display distinct positive europium anomalies, which is indicative of plagioclase accumulation. The mafic and ultramafic rocks generally show incompatible element depleted MORB-normalized trace-element diagrams (Fig. 6d). The contents of incompatible elements in peridotite are lower than the MORB values. The gabbro is relatively enriched in the LILEs (Sr, Rb, Ba, Th) but depleted in incompatible elements. The LILEs in basalt are slightly higher than those in MORB. The trace-element pattern of the basalt is similar to that of tholeiitic and transitional MORB, but is distinctively different from those typical of island-arc basalts (IAB) and/or calc-alkaline basalts (CAB), which are characterized by much larger Nb and Ta minimums (Pearce, 1982).

The diorite, granodiorite and gneissic granite are characterized by slightly higher REE ranging from 60.53 ppm in diorite to 125.88 ppm in gneissic granite. The REE patterns (Fig. 6b) are

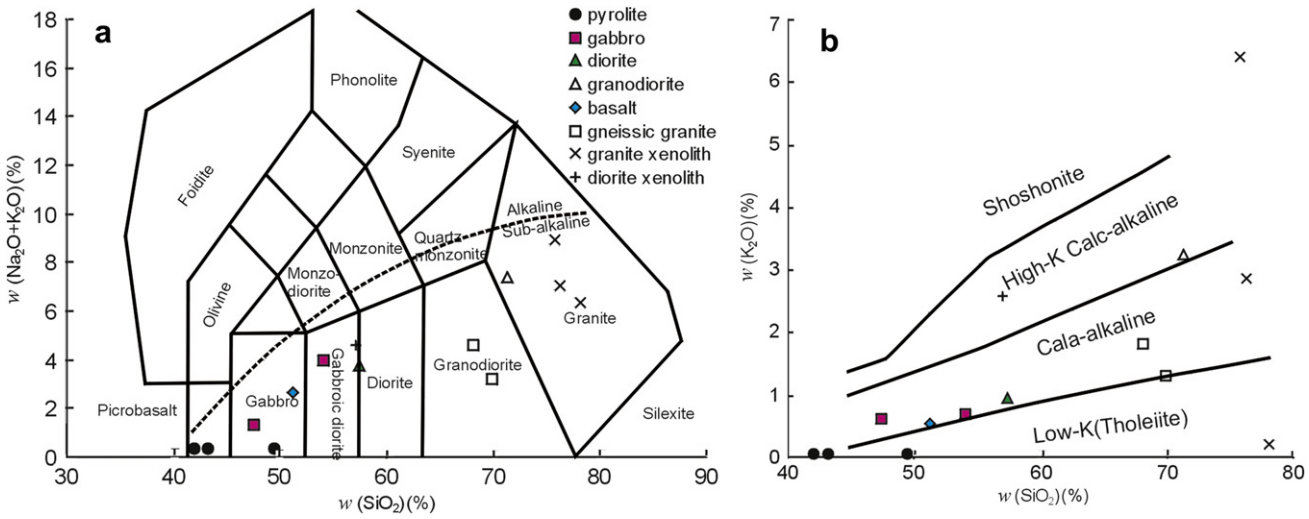

Figure 5 The TAS diagram (a) (after Middlemost, 1994; Irvine and Baragar, 1971) and SiO_2-K_2O diagram (b) (after Ewart, 1982) of various rock types from the Tuerkubantao ophiolitic mélange.

LREE enriched (ΣLREE/ΣHREE > 4) and show undifferentiated HREEs. The REE patterns of these intermediate to felsic rocks possess negative Eu anomalies except for the diorite, which has a positive Eu anomaly similar to that of the gabbro. The MORB-normalized trace-element diagrams (Fig. 6e) of the diorite, granodiorite and gneissic granite are enriched in the LILEs and, to a lesser degree, in medium incompatible elements, but depleted in compatible elements. The concentrations of the LILEs gradually increase from gabbro to diorite, granodiorite and, finally, to gneissic granite possibly indicating an increasing degree of fractional crystallization. The negative Ba anomaly and positive Th anomaly in the trace-element patterns of all samples may result from redox conditions, e.g., in a deep-water environment, or diagenesis.

The ΣREE of the granitoid xenoliths (50–85 ppm) is lower than that of the granodiorite. Their REE patterns are similar to those of the hosting rocks (Fig. 6c), however, the ratios of ΣLREE/ΣHREE in the xenoliths are slightly lower than those in the diorite, granite and gneissic granite. The REE patterns of all xenoliths have negative Eu anomaly, but their δEu values are lower than those in the felsic diorite and granodiorite dykes and in the gneissic granite. The trace-element patterns are enriched in the LILEs but not in other elements (Fig. 6f) and are different to those of the hosting magmatic rocks.

6. Zircon dating

We analyzed zircons from the gabbro, gneissic granite, granitoid xenoliths in gneissic granite and flysch. After crushing the samples and separating zircons using standard methods, we selected representative zircon grains and studied them under a scanning microscope to obtained cathode luminescent and back scattered emission images. The U-Pb dating of zircons was performed in the Research Center of University of Tasmania, Australia (CODES), by using a HP4500 quadrupole ICP-MS equipped with a 213 nm New Type laser ablation machine. Temora standard (Black et al., 2003) and 91500 standard (Wiedenbeck et al., 1995) were used as main and supplementary zircon standards, respectively. The laser beam of 20 μm, 5 Hz and 12 J/cm^2 was limited to an analytical cycle of 0.2 s. The errors were corrected according to the methods of Black et al. (2004) and Harris et al. (2004). The standard error was estimated based on the error of standard samples. The contents of elements were recalculated by a method of Kosler (2001). The results of U-Pb zircon dating are shown in Table 2 and illustrated in Figs. 7 and 8.

Eight zircon grains were analyzed from the gabbro sample K3815-3, among which two zircon grains have coherent internal structures and clear shapes (spots 3 and 8 in Table 2). Cathode luminescence images of the other six grains show inherited cores and oscillatory zoning (Fig. 7a). The cores and rims were analyzed at 14 spots (Table 2). The U-Pb ages of 10 spots are between 351 and 383 Ma, Th/U ranging from 0.25 to 0.98 in most of the spots suggesting their magmatic origin. Except for the 383 Ma age of spot 2, the other nine spots have an average age of 363.8 ± 4.8 Ma (Fig. 8a), i.e., the Late Devonian, which is probably the time of gabbro crystallization. The cores at spots 1, 3, and 10 yielded Pb-Pb ages between 1850 and 1886 Ma, (late Paleoproterozoic), which is probably the age of the crystalline basement.

The U-Pb ages of 14 zircon grains from gneissic granite sample K3815-7-3 range from 350 to 969 and one spot yielded a Pb-Pb age of 2182 Ma (Table 2). Five zircon grains (spots 1, 7, 11, 13 and 14) are of magmatic origin, because they are colorless and transparent, well-shaped, possess oscillatory zoning, Th/U = 0.44–0.72, and the contents of Th and U are positively correlated. The U-Pb ages of these magmatic zircons cluster near the concordia, between 350 and 359 Ma, with an average of 355.4 ± 6.9 Ma, i.e., the probable age of granite crystallization is Late Devonian. The other eight zircon grains (spots 2, 3, 5, 6, 8–10, 12) are also colorless, transparent, well-shaped, possess oscillatory zoning (Fig. 7b), Th/U = 0.18–0.98 and most of the values are between 0.18 and 0.29. Their $^{206}Pb/^{238}U$ ages are discordant ranging from 369 to 969 Ma (Fig. 8b). One zircon grain (spot 4) has an inherited old core with a Pb-Pb age of 2182 Ma, indicating Middle Paleoproterozoic crystalline basement.

Most of the 13 zircon grains from sample K3815-8-1 (diorite xenolith in gneissic granite) are colorless, transparent and well-shaped (Fig. 7c). The Th/U ratios range from 0.31 to 1.26 with the majority higher than 0.4 and the contents of Th and U are well correlated suggesting their magmatic origin. The U-Pb ages of 11 zircons are between 396 and 518 Ma with an average age of

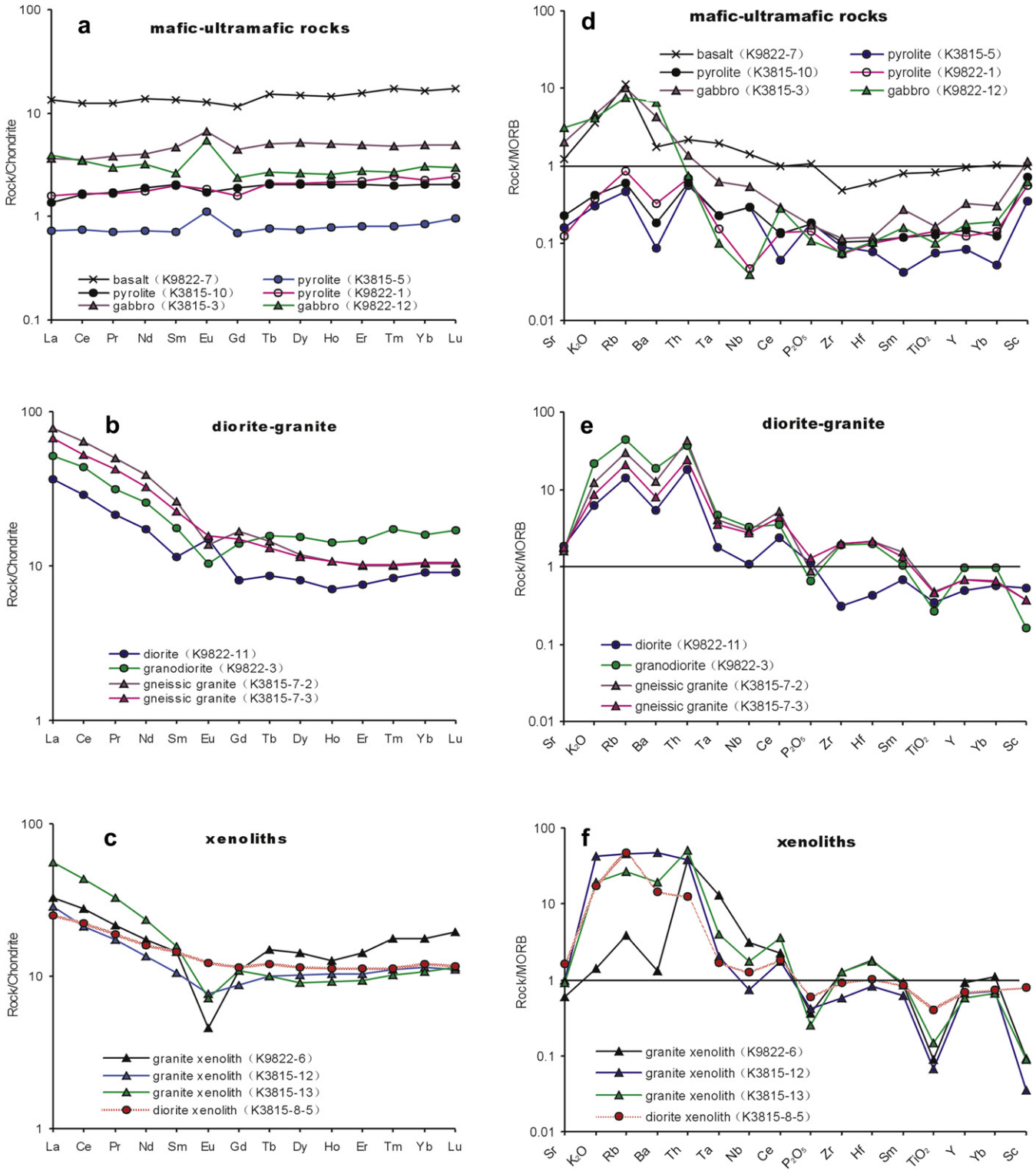

Figure 6 The REE patterns (a, b and c) and trace-element diagrams (d, e and f) of different rock types from the Tuerkubantao ophiolitic mélange. The normalizing values of chondrite and MORB are from Boynton (1984) and Pearce (1982), respectively.

450.5 Ma (Fig. 8c), however the main cluster of ages (seven zircons: spots 2, 5, 6, 7, 9, 11 and 13), which plot near the concordia, is between 369 and 433 Ma with an average age of 430.1 Ma indicating the Early Silurian age of granite crystallization. Two less transparent zircons (spots 8 and 10 in Fig. 7c and Table 2) with Pb-Pb ages of 2632 and 2821 Ma were probably captured from Late Archean basement.

Ten zircon grains from granite xenolith in the flysch layer (K3815-12) were analyzed at 12 spots. Two zircons have inherited cores and transparent rims in CL images (spots 4 and 9 in Fig. 7d,

Table 2 U-Pb data on zircons from rocks of the Tuerkubantao ophiolitic mélange.

	Spot	Th/U	Isotopic age			Isotopic ratio					
			$^{206}Pb/^{238}U$ (Ma)	$^{207}Pb/^{206}Pb$ (Ma)	Discordant (%)	$^{207}Pb/^{206}Pb$	±%	$^{207}Pb/^{235}U$	±%	$^{206}Pb/^{238}U$	±%
Gabbro (K3815-3)	1	0.41	1686 ± 26	1886 ± 29	11	0.1154	1.6	4.808	1.9	0.3036	1.5
	2	0.40	383.0 ± 4.1			0.0541	2.4	0.452	2.4	0.0612	1.1
	3	0.45	1771 ± 16	1853 ± 22	4	0.1133	1.2	4.936	1.3	0.3182	0.9
	4	0.27	1734 ± 17	1867 ± 22	7	0.1142	1.2	4.901	1.3	0.3120	0.9
	5	0.98	364.0 ± 6.5			0.0729	3.6	0.599	4.1	0.0595	1.8
	6	0.39	372.2 ± 5.1			0.0672	3.6	0.555	3.6	0.0604	1.4
	7	0.56	357.8 ± 5.2			0.0595	3.8	0.462	3.7	0.0575	1.4
	8	0.59	363.7 ± 8.0			0.0938	4.4	0.774	4.7	0.0611	2.2
	9	0.25	371.4 ± 8.2			0.0621	4.3	0.506	4.2	0.0599	2.2
	10	0.25	1615 ± 22	1850 ± 31	13	0.1131	1.7	4.550	2.1	0.2899	1.4
	11	0.60	355.8 ± 4.7			0.0637	2.9	0.500	2.9	0.0575	1.3
	12	0.46	365.3 ± 4.0			0.0543	2.1	0.432	2.3	0.0583	1.1
	13	0.41	361.4 ± 4.3			0.0561	3.0	0.438	3.2	0.0578	1.2
	14	0.50	351.4 ± 7.7			0.0913	4.9	0.745	4.6	0.0588	2.2
Gneissic granite (K3815-7-3)	1	0.63	351.4 ± 7.3			0.0608	4.4	0.454	4.9	0.0565	2.1
	2	0.29	369.4 ± 4.6			0.0545	3.2	0.440	3.1	0.0590	1.2
	3	0.20	392.0 ± 5.9			0.0570	4.1	0.484	4.0	0.0629	1.5
	4	0.48	1442 ± 27	2182 ± 31	34	0.1364	1.8	4.972	2.3	0.2665	2.0
	5	0.63	508.5 ± 12.0			0.0665	4.3	0.751	4.6	0.0830	2.4
	6	0.98	396.4 ± 5.8			0.0562	3.5	0.480	3.4	0.0636	1.5
	7	0.46	356.7 ± 6.5			0.0569	5.0	0.430	4.9	0.0571	1.8
	8	0.24	417.4 ± 5.4			0.0590	3.6	0.539	3.7	0.0672	1.3
	9	0.18	388.7 ± 9.7			0.0601	6.7	0.515	7.1	0.0626	2.5
	10	0.43	969.1 ± 21.9	1882 ± 59	49	0.1151	3.3	2.679	3.9	0.1717	2.3
	11	0.44	357.7 ± 5.6			0.0561	4.7	0.435	4.6	0.0572	1.6
	12	0.21	506.2 ± 5.7			0.0621	2.6	0.694	2.7	0.0822	1.1
	13	0.57	358.9 ± 5.1			0.0610	3.9	0.472	3.9	0.0578	1.4
	14	0.72	349.7 ± 4.8			0.0561	4.5	0.416	4.1	0.0559	1.4
Diorite xenolith (K3815-8-1)	1	0.86	518.0 ± 7.0			0.0540	3.7	0.613	3.5	0.0833	1.4
	2	0.77	428.5 ± 9.1			0.0582	5.1	0.553	4.9	0.0690	2.1
	3	1.26	449.1 ± 6.7			0.0536	5.2	0.505	4.5	0.0720	1.5
	4	0.48	511.4 ± 9.0			0.0594	3.5	0.669	3.6	0.0854	1.7
	5	0.31	395.8 ± 5.4			0.0523	3.8	0.448	3.8	0.0631	1.4
	6	0.97	432.7 ± 9.5			0.0570	4.1	0.543	4.2	0.0696	2.2
	7	0.53	424.1 ± 9.1			0.0611	6.9	0.568	6.4	0.0685	2.1
	8	0.79	2741 ± 103	2632 ± 43	−4	0.1778	2.6	12.567	3.8	0.5205	2.8
	9	0.73	431.8 ± 8.3			0.0563	6.8	0.516	6.5	0.0693	1.9
	10	1.10	2412 ± 56	2821 ± 42	14	0.1994	2.6	13.186	2.7	0.4834	1.9
	11	0.56	433.3 ± 8.8			0.0564	7.3	0.535	7.8	0.0725	2.4
	12	0.48	502.1 ± 11.4			0.0567	8.1	0.614	7.4	0.0810	2.3
	13	0.79	430.1 ± 7.3			0.0613	5.4	0.573	5.0	0.0695	1.7
Granite xenolith (K3815-12)	1	0.15	692.8 ± 13.7			0.2509	3.1	5.158	3.4	0.1479	1.4
	2	0.80	424.7 ± 7.8			0.1442	4.4	1.513	4.5	0.0764	1.6
	3	0.90	423.1 ± 5.8			0.0744	3.8	0.697	3.4	0.0695	1.4
	4	0.80	467.9 ± 18.5			0.4665	2.2	9.894	3.4	0.1515	2.0
	5	0.35	417.2 ± 7.6			0.1843	3.2	2.033	3.9	0.0794	1.6
	6	0.44	447.2 ± 10.9			0.2440	3.6	3.196	4.4	0.0934	1.9
	7	0.55	430.6 ± 7.2			0.1122	3.3	1.134	3.5	0.0742	1.6
	8	0.78	419.3 ± 9.9			0.3501	2.0	5.092	2.5	0.1052	1.4
	9	0.25	800.9 ± 12.7			0.1724	2.7	3.612	3.0	0.1525	1.4
	10	0.94	423.0 ± 6.6			0.1043	3.2	1.031	3.2	0.0721	1.5
	11	0.67	424.9 ± 7.8			0.0935	5.0	0.943	5.7	0.0715	1.8
	12	0.36	417.2 ± 9.1			0.2699	2.2	3.358	2.7	0.0907	1.8

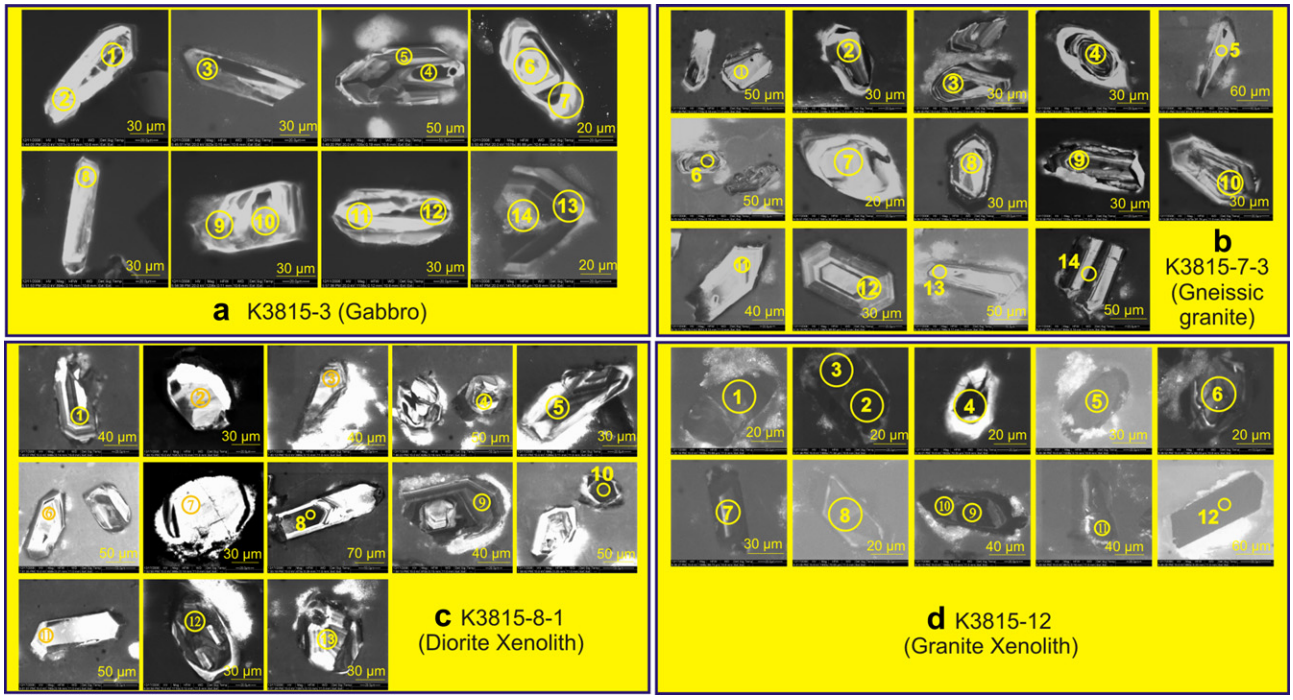

Figure 7 The CL images of zircons from the Tuerkubantao rocks. The host rocks (a-gabbro, b-gneissic granite, c-diorite xenolith and d-granite xenolith) and their sample numbers, analytical spots and numbers are marked.

respectively). The U-Pb ages of the cores are 469 and 801 Ma (Fig. 8d). The rest CL images show 10 dark gray zircons with relatively high contents of Th, U and Pb (Table 2). Most of the zircons are characterized by Th/U in the range from 0.35 to 0.94 and positively correlated Th and U, suggesting their magmatic origin, except for spot 1 in zircon with micro-fractures and relatively low Th/U (0.15). The U-Pb ages of these zircons are from 417 to 447 Ma with an average of 425.6 ± 6.1 Ma, i.e., the Middle Silurian.

7. Discussion

7.1. Tectonic setting and age of Tuerkubantao rocks

The flat trace-element patterns of the mafic-ultramafic rocks suggest their affinity to ophiolites. The basalts are associated with mafic-ultramafic rocks of the ophiolite assemblage. They possess flat REE and trace-element patterns ($La/Sm_n = 1.00$; $La/Yb_n = 0.82$; $Th/Nb_{pm} = 0.56$; $La/Nb_{pm} = 0.73$), which suggest their formation in a mid-ocean ridge setting (Fig. 6a and d).

The granodiorite and gneissic granite fall in the field of volcanic arc granite or syn-COLG in the discriminating tectonic diagram (Table 3, diagrams not shown). In the R_1-R_2 diagram, these rocks plot close to mantle granite. As the gneissic granite occurs within the zone of strong deformation and contains numerous xenoliths, we suggest that it formed in a subduction setting simultaneously with the emplacement of ophiolites.

The tectonic setting of formation of granitic and diorite xenoliths is more complex. In the R_1-R_2 diagram, the diorite xenoliths in basaltic rocks mainly fall into the field of volcanic arc granite, i.e., formed in a pre-collision subduction-related setting. The environment and time of their formation were possibly similar to those of gneissic granite. Two granite xenoliths (K3815-12, K3815-13) possess chemical affinities of volcanic arc or syn-collision granite, suggesting their formation in an early magmatic arc setting. Another granite xenolith sample (K9822-6) plots into the fields of within-plate, ocean ridge and mantle granitoids in different tectonic discrimination diagrams. Based on the known Paleozoic ophiolite and trench-arc-basin system in the northern Altay (Wang et al., 1998), we consider that this granite xenolith might be a product of the same magmatic event as recorded in the northern Chinese Altay.

The 363 Ma isotopic age of gabbro indicates that the Tuerkubantao ophiolitic unit formed in the Late Devonian. The subduction-related tectonic setting of granite formation and the 355 Ma age of gneissic granite may indicate the Late Devonian to Early Carboniferous ophiolite subduction. The Late Silurian age of Tuerkubantao granite and diorite xenoliths (425–430 Ma) corresponds to the 390–441 Ma age of granites exposed in the Chonghuer area of the Chinese Altay (Sun et al., 2009). The 2632 and 2821 Ma inherited zircons from granite xenoliths could have been captured from the Altay crystalline basement, because the Junggar terrane is thought to be an "immature" massif lacking Precambrian basement (Wang et al., 2004), or recycled.

7.2. Extension of the Tuerkubantao ophiolite

There are three fault-bounded and sheared ophiolite belts in the eastern Kekesentao area, Kuerti, Qiaoxiahala-Buergen and Zhaheba-Aermantai (from north to south), which contain ophiolitic mélange. There are two schemes for linking the Kekesentao ophiolite belt with other ophiolites. The first scheme of Kekesentao-Zhaheba-Aermantai was proposed by early researchers (He et al., 1990; Chen et al., 1993; Shu et al., 2001). The second scheme of Kekesentao-Qiaoxiahala-Buergen was proposed in recent studies (Wu et al., 2006; Wang et al., 2003). We prefer the second scheme based on an evaluation of the geological, geochemical and geochronological data (Table 4).

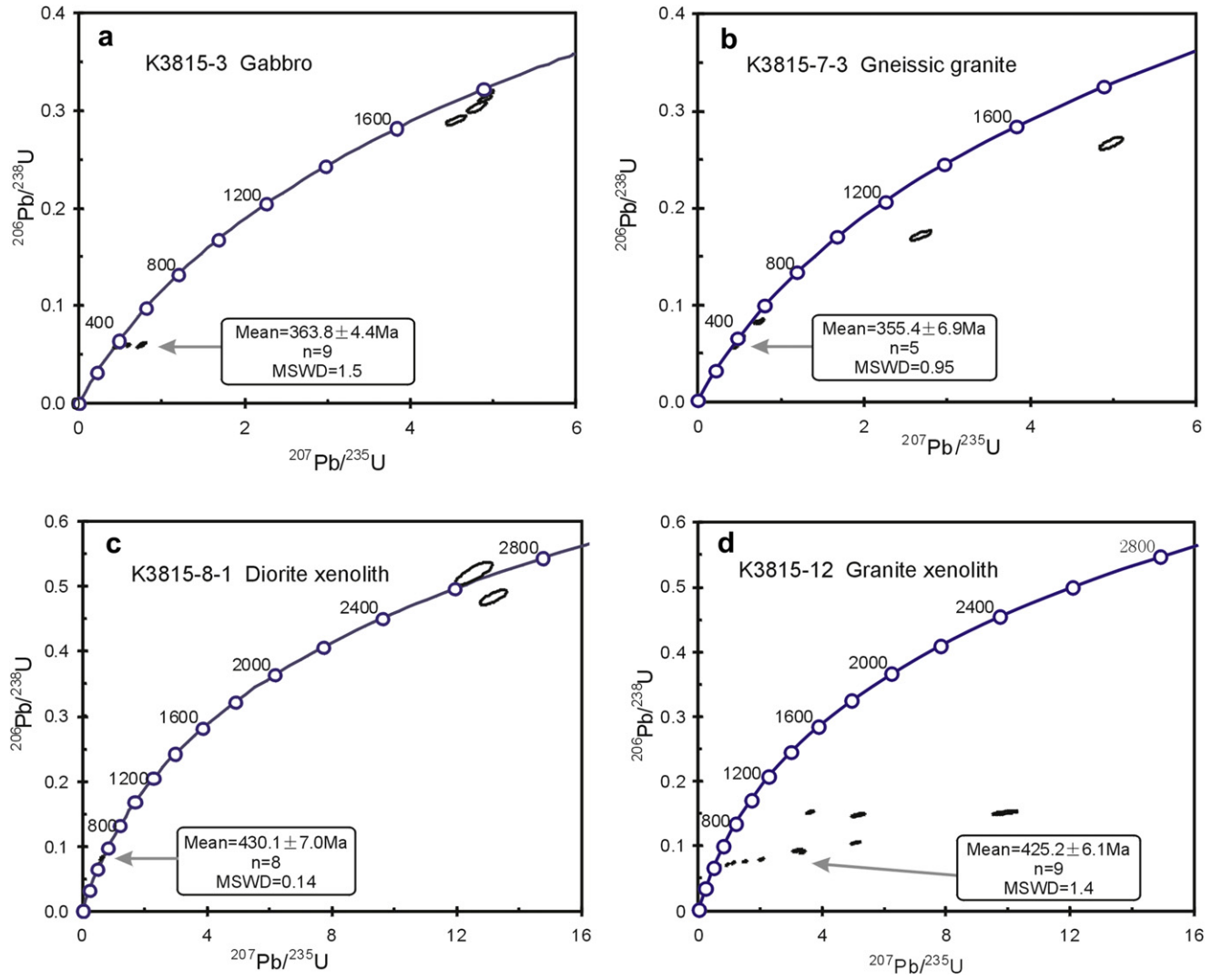

Figure 8 The U-Pb concordia of zircons from the Tuerkubantao ophiolitic mélange. The host rocks (a-gabbro, b-gneissic granite, c-diorite xenolith and d-granite xenolith) and their sample numbers are marked.

A possible eastern continuation of the Kekesentao ophiolite can be the Bidz ophiolite in southwestern Mongolia, which extends from NW to SE to a distance of more than 1000 km as a narrow sliver (Badarch et al., 2002). The Bidz ophiolite consists of tholeiitic pillow basalts, tuffs, cherts, sandstones, siltstones, argillites, and minor thin layers of limestones, intruded by gabbros and diorites. The Devonian age of volcanic and sedimentary rocks is based on regional correlations (Ruzhentsev and Pospelov, 1992; He and Li, 2000; Wu et al., 2006), because no high-resolution isotopic ages have been obtained for these rocks so far. Major and rare earth element data suggest that Bidz basalts are MORB-type and formed in a mid-oceanic ridge setting (Ruzhentsev and Pospelov, 1992; Ruzhentsev and Mossakovskiy, 1996). Therefore, we believe that the Bidz ophiolite can be correlated with the Kekesentao-Buergen ophiolite zone (Windley et al., 1994; Wu et al., 2006; Xiao et al., 2009).

Table 3 Tectonic settings of formation of Tuerkubantao granitoids.

Discrimination diagram	Granodiorite	Gneissic granite	Granite xenolith	Diorite xenolith
Nb-Y diagram	VAG + syn-COLG	VAG + syn-COLG	VAG + syn-COLG	VAG + syn-COLG
Ta-Yb diagram	VAG	VAG	VAG, WPG	VAG
Rb-(Y + Nb) diagram	VAG	VAG	VAG, ORG	VAG
Rb-(Yb + Ta) diagram	VAG	VAG	VAG	VAG
Rb/10-Hf-3*Ta diagram	VAG	VAG	VAG, WPG	VAG
Rb/30-Hf-3*Ta diagram	VAG	VAG	VAG, WPG	VAG
R_1-R_2 diagram	syn-COLG	MG	syn-COLG, MG	Pre-COLG

Abbreviations: ORG – ocean ridge granite; syn-COLG – syn-collision granite; VAG – volcanic arc granite; WPG – within-plate granite; Pre-COLG – pre-collision (subduction zone) granite; MG – mantle granite.

Table 4 Comparison between the Tuerkubantao and adjacent ophiolites.

Ophiolite geology	Tuerkubantao	Kuerti	Buergen	Aermantai
Rock association	Ultramafic, gabbro, diorite, granodiorite, basalt	Basalt, gabbro, diabase	Altered ultramafic, gabbro, basalt	Ultramafic, gabbro, plagiogranite, diabase, andesite, basalt
Ultramafic rocks	Lherzolite, peridotite		Altered ultramafic	Altered peridotite, harzburgite, lherzolite
Basalt types	Low-Ti tholeiite	Low-K, Ti tholeiite	Tholeiite	Andesitic to felsic volcanoclastic rocks
Associated sediments	Flysch formation, siliceous rocks	Siliceous rocks	Siliceous rocks	Cherts, flysch and limestones
U-Pb dating (zircon)	363.8 ± 4.8 Ma (gabbro)	372 ± 19 Ma (plagiogranite)	352.1 ± 4.4 Ma (basalt)	503 ± 7 Ma (plagiogranite)
Tectonic setting	MORB	Back-arc basin	OIB, IAB	IAB
References	This work	Xu et al., 2001, 2003; Zhang et al., 2003a	Wu et al., 2006	Huang et al., 1997; Wang et al., 2003; Xiao et al., 2006b

Abbreviations: MORB – mid-ocean ridge basalt; OIB – oceanic island basalt; IAB – island-arc basalt.

A possible western continuation of the Kekesentao ophiolite zone could be the Char ophiolite belt in East Kazakhstan, which is also a suture-shear zone hosting Late Devonian oceanic basalts (Buslov et al., 2001, 2004; Safonova et al., 2004, 2012). The Char belt comprises three types of serpentine mélanges: (i) Early Paleozoic subduction mélange including meta-gabbro, meta-basalt, metamorphosed deep-water siliceous sediments, eclogites, amphibolites and glaucophane schists; (ii) Ordovician ophiolitic mélange containing blocks of oceanic basaltic lavas and layers of siliceous mudstone and chert; (iii) Late Carboniferous–Early Permian mélange separating tectonic sheets (Dobretsov et al., 1992; Iwata et al., 1996; Buslov et al., 2001, 2004). Unfortunately, no high-resolution isotopic ages have been reported yet. However, the OPS (oceanic plate stratigraphy) units occur in both types (i) and (ii) mélanges and contain Middle Devonian–Early Carboniferous radiolarians and conodonts (Iwata et al., 1996; Buslov et al., 2001), which accords well with the age of the Tuerkubantao gabbro. Furthermore, the co-occurrence of mafic-ultramafic rocks, low-Ti tholeiitic basalts and mid-oceanic ridge basalts in the Char ophiolite belt or suture-shear zone (Polyansky et al., 1979; Buslov et al., 2001; Safonova et al., 2012) is similar to that present in the Tuerkubantao ophiolitic mélange.

7.3. Implications for the tectonic evolution of Central Asia

The southern Altaids record a long and multi-stage oceanic evolution and accretionary history since the Early Paleozoic. The opening of the Paleo-Asian Ocean probably began in the Neoproterozoic (970–850 Ma, Dobretsov et al., 1995, 2003), and then the ocean underwent at least five important geodynamic stages (Buslov et al., 2001). There are several different views on the timing of the final closure of the Paleo-Asian Ocean: Early-Middle Devonian (Wang et al., 1990; Han et al., 1997), Late Devonian-Early Carboniferous (Windley et al., 1990; Allen et al., 1993; Gao et al., 1995; Buslov et al., 2001; Li et al., 2006b; Zhang et al., 2008a), or Permian (Sun et al., 1991; Xiao et al., 2006a, 2008).

The data presented in this paper indicate that the time of the final subduction is post-Middle Devonian. The 363 Ma age of the MORB-type gabbro and the 355 Ma age of the gneissic granite may correspond to the subduction of the Ob'-Zaisan Ocean crust beneath an active margin of the Siberian continent, prior to its collision with the Kazakhstan continent in Late Devonian–Early Carboniferous time (Iwata et al., 1996; Buslov et al., 2001, 2004; Safonova et al., 2012). Taking into account the pre-Early Carboniferous age of the Kekesentao ophiolite, the Late Carboniferous age of the intracontinental volcanic Batamayineishan Formation in the Junggar area (Zhang et al., 2009), and the Middle-Late Carboniferous age of the Ulungur A-type alkali granites in eastern Junggar (293–320 Ma, Wang et al., 1994; Liu and Yuan, 2006), we accept that the final closure of the Paleo-Asian Ocean was after the Late Carboniferous but before the Early Permian.

8. Conclusions

An ophiolitic mélange containing ultramafic rocks, gabbro, diabase, basalt and flysch formation occurs in the Tuerkubantao district of the Kekesentao area, northern Xinjiang. The mafic-ultramafic rocks and basalts belong to the tholeiitic series and are characterized by low alkali, low TiO_2 and high MgO. The basalts are geochemically similar to MORB, i.e., formed in a mid-oceanic ridge setting. The high-Na and low-K gneissic granite was formed in volcanic arc or syn-collision tectonic settings as a result of oceanic crust subduction. The U-Pb zircon age of gabbro and gneissic granite is from 363 Ma to 355 Ma, indicating that the formation of ophiolite mélange or the subduction of oceanic crust was during the Late Devonian.

The Kekesentao ophiolite, together with the Qiaoxiahala and Buergen ophiolites form an ophiolitic mélange zone along the Erqis fault, which western continuation is the Char ophiolite zone in East Kazakhstan and eastern continuation is the Bidz ophiolite zone in southwestern Mongolia. All these ophiolitic belts are part of the Zaisan (Char)-Kekesentao-South Mongolia geosuture zone separating the Siberian and Kazakhstan continents.

Acknowledgments

This work was supported by the Major State Basic Research Program of the People's Republic of China (Nos. 2007CB411304

and 2001CB409806). The authors are grateful to Dr. Inna Safonova, Associate Editor of Geoscience Frontiers, for careful editing of the manuscript and suggestions for revision and to an anonymous reviewer for helpful comments.

References

Allen, M.B., Windley, B.F., Zhang, C., 1993. Palaeozoic collisional tectonics and magmatism of the Chinese Tien Shan, central Asia. Tectonophysics 220, 89–115.

Badarch, G., Cunningham, W.D., Windley, B.F., 2002. A new terrane subdivision for Mongolia: implications for the Phanerozoic crustal growth of Central Asia. Journal of Asian Earth Sciences 21, 87–110.

Black, L.P., Kamo, S.L., Allen, C.M., Aleinikoff, J.N., Davis, D.W., Korsch, R.J., Foudoulis, C., 2003. TEMORA 1: a new zircon standard for Phanerozoic U-Pb geochronology. Chemical Geology 200, 155–170.

Black, L.P., Kamo, S.L., Allen, C.M., Davis, D.W., Aleninikoff, J.N., Valley, J.W., Mundil, R., Campbell, I.H., Korsch, R.J., Williams, I.S., Foudoulis, C., 2004. Improved $^{206}Pb/^{238}U$ microprobe geochronology by the monitoring of a trace-element related matrix effect; SHRIMP, ID-TIMS, ELA-ICP-MS, and oxygen isotope documentation for a series of zircon standards. Chemical Geology 205, 115–140.

Bloomer, S.H., Stern, R.J., Smoot, N.C., 1989. Physical volcanology of the submarine Mariana and Volcano Arcs. Bulletin of Volcanology 51, 210–224.

Boynton, W.V., 1984. Cosmochemistry of the rare earth elements: meteorite studies. Developments in Geochemistry 2, 63–114.

Buslov, M.M., Safonova, I.Y., Watanabe, T., Obut, O., Fujiwara, Y., Iwata, K., Semakov, N.N., Sugai, Y., Smirnova, L.V., Kazansky, A.Y., 2001. Evolution of the Paleo-Asian Ocean (Altai-Sayan region, Central Asia) and collision of possible Gondwana-derived terranes with the southern marginal part of the Siberian continent. Geosciences Journal 5, 203–224.

Buslov, M.M., Watanabe, T., Fujiwara, Y., Iwata, K., Smirnova, L.V., Safonova, I.Y., Semakov, N.N., Kiryanova, A.P., 2004. Late Paleozoic faults of the Altai region, Central Asia: tectonic pattern and model of formation. Journal of Asian Earth Sciences 23, 655–671.

Cao, R.L., 1994. The ophiolite of North Xinjiang and its basic-ultrabasic complex. Xinjiang Geology 12 (1), 25–31 (in Chinese with English abstract).

Chen, Z.F., Chen, S.D., Liang, Y.H., Xu, X., 1997. Opening-closing Tectonics of Xinjiang and Mineralization. Xinjiang Technology and Sanitation Press, Urumqi, 156 pp (in Chinese with English abstract).

Chen, Z.F., Xu, X., Liang, Y.H., 1993. The basic features of the accordion-style opening-closing evolution of structures in Xinjiang. Regional Geology of China 1, 45–58 (in Chinese with English abstract).

Coleman, R.G., 1977. Ophiolites, Ancient Oceanic Lithosphere? Springers-Verlag, Berlin, pp. 78–123.

Dharma Rao, C.V., Santosh, M., Wu, Y.-B., 2011. Mesoproterozoic ophiolitic mélange from the SE periphery of the Indian plate: U-Pb zircon ages and tectonic implications. Gondwana Research 19, 384–401.

Dobretsov, N.L., Berzin, N.A., Buslov, M.M., 1995. Opening and tectonic evolution of the Paleo-AsianOcean. International Geology Review 37, 335–360.

Dobretsov, N.L., Buslov, M.M., Vernikovsky, V.A., 2003. Neoproterozoic to Early Ordovician evolution of the Paleo-AsianOcean: implications to the break-up of Rodinia. Gondwana Research 6, 143–159.

Dobretsov, N.L., Simonov, V.A., Buslov, M.M., Kurenkov, S.A., 1992. Oceanic and island-arc ophiolites of Gorny Altai. Russian Geology and Geophysics 12, 3–14.

Dong, L.H., Zhu, Z.X., Qu, X., Wang, K.Z., Zhao, T.Y., 2010. Spatial distribution, geological features and latest research progress of the main ophiolite zones in Xinjiang, NW-China. Acta Petrologica Sinica 26 (10), 2894–2904 (in Chinese with English abstract).

Dong, X.Y., Li, H., Ye, L.Z., Li, J.M., Zheng, J.T., Wang, S.S., Yang, X.Z., Zhao, D.H., 1995. Ultramafic Rocks in China. Geological Publishing House, Beijing, 329 pp (in Chinese with English abstract).

Ewart, A., 1982. The mineralogy and petrology of Tertiary-Recent orogenic volcanic rocks with special reference to the andesitic-basaltic compositional range. In: Thorpe, R.S. (Ed.), Andesites. Wiley, Chichester, pp. 25–87.

Gao, J., He, G.Q., Li, M.S., Xiao, X.C., Tang, Y.Q., 1995. The mineralogy, petrology, metamorphic PTDt trajectory and exhumation mechanism of blueschists, south Tianshan, northwestern China. Tectonophysics 250, 151–168.

Glorie, S., De Grave, J., Buslov, M.M., Zhimulev, F.I., Izmer, A., Vandoorne, W., Ryabinin, A., Van den haute, P., Vanhaecke, F., Elburg, M.A., 2011. Formation and Palaeozoic evolution of the Gorny-Altai Mongolia suture zone (South Sibera): Zircon U/Pb constraints on the igneous record. Gondwana Research 20, 465–484.

Gribble, R.F., Bloomer, S.H., Stuben, D., Ohearn, T., Newman, S., Stern, R.J., 1996. MORB mantle and subduction components interact to generate basalts in the southern Mariana Trough back-arc basin. Geochemica et Cosmochimica Acta 60, 2153–2166.

Han, B.F., Wang, S.G., Jahn, B.M., Hong, D.W., Kagami, H., Sun, Y., 1997. Depleted mantle source for the Ulungur River A-type granites from North Xinjiang, China: geochemistry and Nd-Sr isotopic evidence, and implications for the Phanerozoic crustal growth. Chemical Geology 138, 135–159.

Harris, A.C., Allen, C.M., Bryan, S.E., Campbell, I.H., Holcombe, R.J., Palin, J.M., 2004. ELA-ICP-MS U-Pb zircon geochronology of regional volcanism hosting the Bajo de la Alumbrera Cu-Au deposit: implications for porphyry-related mineralization. Mineralium Deposita 39, 46–67.

He, G.Q., Han, B.F., Yue, Y.J., Wang, J.H., 1990. Tectonic Division and Crustal Evolution of Altay Orogenic Belt in China. Geoscience of Xinjiang. Geological Publishing House, Beijing, pp. 9–22 (in Chinese with English abstract).

He, G.Q., Li, M.S., 2000. New achievement in researching ophiolitic belts in central Asia and its significance in the links of tectonic belts between Northern Xinjiang and adjacent area. Xinjiang Geology 18 (3), 193–202 (in Chinese with English abstract).

He, G.Q., Li, M.S., Liu, D.Q., Tang, Y.L., Zhou, R.H., 1994. The Crust Evolution and its Mineralization of the Paleozoic Era, Xinjiang, China. Xinjiang People's Publishing House, Urumqi, 437 pp (in Chinese with English abstract).

Huang, X., Jin, C.W., Sun, B.S., Pan, J., Zhang, R.H., 1997. Study on the age of Aermantai ophiolite, Xinjiang by Nd-Sr isotope geology. Acta Mathematica Sinica 13, 85–91 (in Chinese with English abstract).

Irvine, T.N., Baragar, W.R.A., 1971. A guide to the chemical classification of the common volcanic rocks. Canadian Journal of Earth Sciences 8, 523–548.

Iwata, K., Obut, O.T., Buslov, M.M., 1996. Devonian and Lower Caboniferous radiolarians from the Chara ophiolite belt, East Kazakhstan. News of Osaka Micropaleontologist 10, 27–32.

Jahn, B.M., Windley, B., Natal'in, B., Dobretsov, N., 2004. Phanerozoic continental growth in Central Asia. Journal of Asian Earth Sciences 23, 599–603.

Kosler, J., 2001. Laser-ablation ICPMS study of metamorphic minerals and processes. In: Sylvester, P.J. (Ed.), Laser-ablation-ICPMS in the Earth Sciences: Principles and Applications. Mineralogical Association of Canada Short Course Handbook 29, pp. 185–202.

Laurent-Charvet, S., Charvet, J., Monie, P., Shu, L., 2003. Late Paleozoic strike-slip shear zones in eastern central Asia (NW China): new structural and geochronological data. Tectonics 22, 1009.

Li, C.Y., Wang, Q., Liu, X.Y., Tang, Y.Q., 1982. Map of Tectonics of Asia (1: 8000000) and the Notebook. Atlas Publishing House, Beijing.

Li, J.Y., He, G.Q., Xu, X., Li, H.Q., Sun, G.H., Yang, T.N., Gao, L.M., Zhu, Z.X., 2006a. Crustal tectonic framework of northern Xinjiang and adjacent regions and its formation. Acta Geologica Sinica 80 (1), 148–168 (in Chinese with English abstract).

Li, J.Y., Wang, K.Z., Sun, G.H., Mo, S.G., Li, W.Q., Yang, T.N., Gao, L.M., 2006b. Paleozoic active margin slices in the southern Turfan-Hami basin: geological records of subduction of the Paleo-AsianOcean plate in central Asian regions. Acta Petrologica Sinica 22 (5), 1087−1102 (in Chinese with English abstract).

Liu, F.B., 1983. Altay paleo-plate and its endogenetic mineral depostite. Northwestern Geology 4, 14−21 (in Chinese).

Liu, J.Y., Yuan, K.R., 2006. A discussion on the genesis and tectonic setting of alkali granites in the Ulungur alkali-rich granite belt, Xinjiang. Geological Journal of China Universities 2 (3), 257−272.

Long, X., Yuan, C., Sun, M., Safonova, I., Xiao, W., Wang, Y., 2012. Geochemistry and U-Pb detrital zircon dating of Paleozoic graywackes in East Junggar, NW China: insights into subduction-accretion process in the southern Central Asian Orogenic Belt. Gondwana Research 21, 637−653.

Ma, R.S., Shu, L.S., Sun, J., 1997. Tectonic Evolution and Metallogeny of Eastern Tianshan Mountains. Geological Publishing House, Beijing, 202 pp (in Chinese with English abstract).

Middlemost, E.A.K., 1994. Naming materials in the magma/igneous rocks system. Earth Science Reviews 37, 215−224.

Niu, H.C., Sato, H., Zhang, H.X., Ito, J.I., Yu, X.Y., Nagao, T., Terada, K., Zhang, Q., 2006. Juxtaposition of adakite, bininite, high-TiO_2 and low-TiO_2 basalts in the Devonian southern Altai, Xinjiang, NW China. Journal of Asian Earth Sciences 28, 439−456.

Niu, H.C., Xu, J., Yu, X.Y., Chen, F.R., Zheng, Z.P., 1999. Discovery of the Mg-rich volcanics in Altay, Xinjiang, and its geological implications. Chinese Science Bulletin 44, 1685−1688.

Pearce, J.A., 1982. Trace element characteristics of lavas from destructive plate boundaries. In: Thorpe, R.S. (Ed.), Andesites. Wiley, Chichester, pp. 525−548.

Pearce, J.A., Lippard, S.J., Roberts, S., 1984. Characteristics and tectonic significance of super-subduction zone ophiolites. In: Kokelaar, B.P., Howells, M.F. (Eds.), Marginal Basin Geology. Geological Society Special Publication 16, pp. 77−94.

Pirajno, F., Seltmann, R., Yang, Y., 2011. A review of mineral systems and associated tectonic settings of northern Xinjiang, NW China. Geoscience Frontiers 2, 157−185.

Polyansky, N.V., Dobretsov, N.L., Ermolov, P.V., Kuzebny, V.S., 1979. Structure and evolutionary history of the Chara ophiolite belt. Geology and Geophysics 5, 66−78.

Ren, J.S., Jiang, C.F., Zhang, Z.K., Qin, D.Y., 1980. Geotectonic Evolution of China. Science Press, Beijing, 124 pp (in Chinese).

Rippington, S., Cunningham, D., England, R., 2008. Structure and petrology of the Altan Uul ophiolite: new evidence for a Late Carboniferous suture in the Gobi Altai, southern Mongolia. Journal of the Geological Society, London 165, 711−723.

Ruzhentsev, S.V., Mossakovskiy, A.A., 1996. Geodynamics and tectonic evolution of the Central Asian Paleozoic structures as the result of the interaction between the Pacific and Indo-Atlantic segments of the Earth. Geotectonics 29, 294−311.

Ruzhentsev, S.V., Pospelov, I.I., 1992. The southern Mongolian Variscan fold system. Geotectonics 26, 383−395.

Safonova, I.Y., Buslov, M.M., Iwata, K., Kokh, D.A., 2004. Fragments of Vendian-Early Carboniferous oceanic crust of the Paleo-Asian Ocean in foldbelts of the Altai-Sayan region of Central Asia: geochemistry, biostratigraphy and structural setting. Gondwana Research 7, 771−790.

Safonova, I.Yu., Utsunomiya, A., Kojima, S., Nakae, S., Koizumi, K., Tomurtogoo, O., Filippov, A.N., 2009. Pacific superplume-related oceanic basalts hosted by accretionary complexes of Central Asia, Russian Far East and Japan. Gondwana Research 16, 587−608.

Safonova, I.Y., Seltmann, R., Kroener, A., Gladkochub, D., Schulmann, K., Xiao, W., Kim, T., Komiya, T., Sun, M., 2011. A new concept of continental construction in the Central Asian Orogenic Belt (compared to actualistic examples from the Western Pacific). Episodes 34, 186−194.

Safonova, I.Y., Simonov, V.A., Obut, O.T., Kurganskaya, E.V., Romer, R., Seltmann, R., 2012. Late Paleozoic oceanic basalts hosted by the Char suture-shear zone, East Kazakhstan: geological position, geochemistry, petrogenesis and tectonic setting. Journal of Asian Earth Sciences. doi: 10.1016/j.jseaes.2011.11.015.

Sengör, A.M.C., Natal'in, B.A., Burtman, V.S., 1993. Evolution of the Altaid tectonic collage and Paleozoic crustal growth in Eurasia. Nature 364, 299−307.

Shu, L.S., Lu, H.F., Yin, D.H., Ma, R.S., Charvet, J., Laurent-Charvet, S., 2001. Late Paleozoic continental accretionary tectonics in northern Xinjiang. Xinjiang Geology 19 (1), 59−63 (in Chinese with English abstract).

Stern, R.J., Bloomer, S.H., Lin, P.H., Smoot, N.C., 1989. Submarine arc volcanism in the southern Mariana Arc as an ophiolite analogue. Tectonophysics 168, 151−170.

Sun, M., Long, X.P., Cai, K.D., Jiang, Y.D., Wang, B.Y., Yuan, C., Zhao, G.C., Xiao, W.J., Wu, F.Y., 2009. Early Paleozoic ridge subduction in the Chinese Altai: insight from the abrupt change in zircon Hf isotopic compositions. Science in China (Series D) 39 (7), 935−948 (in Chinese).

Sun, S., Li, J.L., Lin, J.L., Wang, Q.C., Chen, H.H., 1991. Indosinides in China and the consumption of Eastern Paleotethys. In: Muller, D.W., McKenzie, J.A., Weissert, H. (Eds.), Controversies in Modern Geology. Academic Press, London, pp. 363−384.

Wang, D.Z., Zhou, X.M., 1982. Volcanic Petrology. Science Press, Beijing, 244 pp (in Chinese).

Wang, J.B., Li, B.Q., Zhang, J.B., Yin, Y.Q., Wang, J.S., Wang, Z.Y., Zheng, G.H., 1999. Copper and Gold Metallogenetic Condition and Prospect Prognosis of the Irtys Ore Belt. Metallurgical Industry Press, Beijing, 178 pp (in Chinese).

Wang, J.B., Qin, K.Z., Wu, Z.L., Hu, J.H., Deng, J.N., Zhang, J.H., Bian, Y.G., Li, S.Q., 1998. Volcanic-Exhalative-Sedimentary Lead-Zinc Deposits in the Southern Margin of the Altay, Xinjiang. Geological Publishing House, Beijing, 210 pp (in Chinese with English abstract).

Wang, J.B., Wang, Y.W., Wang, L.J., 2004. The Junggar immature continental crust province and its mineralization. Acta Geologica Sinica 78 (2), 337−344.

Wang, J.B., Xu, X., 2006. Post-collisional tectonic evolution and metallogenesis in Northern Xinjiang, China. Acta Geologica Sinica 80 (1), 23−31 (in Chinese with English abstract).

Wang, S.G., Han, B.F., Hong, D.W., Xu, B.L., Sun, Y.Y., 1994. Geochemistry and tectonic significance of alkali granites along Ulungur River, Xinjiang. Scientia Geologica Sinica 29 (4), 373−383 (in Chinese with English abstract).

Wang, Z.H., Sun, S., Li, J.L., Hou, Q.L., Qin, K.Z., Xiao, W.J., Hao, J., 2003. Paleozoic tectonic evolution of the northern Xinjiang, China: geochemical and geochronological constraints from the ophiolites. Tectonics 22, 1014. doi:10.1029/2002TC001396.

Wang, Z.X., Wu, J.Y., Liu, C.D., Lu, X.C., Zhang, J.G., 1990. Polycyclic Tectonic Evolution and Metallogeny of the Tianshan Mountains. Science Press, Beijing, 29−37 (in Chinese).

Wiedenbeck, M., Alle, P., Corfu, F., Griffin, W.L., Meier, M., Oberli, F., Vonquadt, A., Roddick, J.C., Speigel, W., 1995. 3 natural zircon standards for U-Th-Pb, Lu-Hf, trace-element and REE analyses. Geostandards Newsletter 19, 1−23.

Windley, B.F., Allen, M.B., Zhang, C., Zhao, Z.Y., Wang, G.R., 1990. Paleozoic accretion and Cenozoic redeformation of the Chinese Tien Shan Range, Central Asia. Geology 18, 128−131.

Windley, B.F., Guo, J.H., Zhang, C., 1994. Subdivision and tectonic evolution of the Chinese Altay. Russian Geology and Geophysics 35, 116−117.

Wu, B., He, G.Q., Wu, T.R., Li, H.J., Luo, H.L., 2006. Discovery of the Buergen ophiolitic mélange belt in Xinjiang and its tectonic significance. Geology in China 33 (3), 476−486 (in Chinese with English abstract).

Xiao, W.J., Han, C.M., Yuan, C., Chen, H.L., Sun, M., Lin, S.F., Li, Z.L., Mao, Q.G., Zhang, J.E., Sun, S., Li, J.L., 2006a. The unique Carboniferous-Permian tectonic-metallogenic framework of Northern Xinjiang (NW China): constraints for the tectonics of the southern

Paleoasian Domain. Acta Petrologica Sinica 22, 1362−1376 (in Chinese with English abstract).

Xiao, W.J., Han, C.M., Yuan, C., Sun, M., Lin, S.F., Chen, H.L., Li, Z.L., Li, J.L., Sun, S., 2008. Middle Cambrian to Permian subduction-related accretionary orogenesis of Northern Xinjiang, NW China: implications for the tectonic evolution of central Asia. Journal of Asian Earth Sciences 32, 102−117.

Xiao, W.J., Windley, B.F., Badarch, G., Sun, S., Li, J.L., Qin, K.Z., Wang, Z.H., 2004. Palaeozoic accretionary and convergent tectonics of the southern Altaids: implications for the lateral growth of Central Asia. Journal of the Geological Society, London 161, 339−342.

Xiao, W.J., Windley, B.F., Yan, Q.R., Qin, K.Z., Chen, H.L., Yuan, C., Sun, M., Li, J.L., Sun, S., 2006b. SHRIMP zircon age of the Aermantai ophiolite in the North Xinjiang, China and its tectonic implications. Acta Geologica Sinica 80, 32−36 (in Chinese with English abstract).

Xiao, W.J., Windley, B.F., Yuan, C., Sun, M., Han, C.M., Lin, S.F., Chen, H.L., Yan, Q.R., Liu, D.Y., Qin, K.Z., Li, J.L., Sun, S., 2009. Paleozoic multiple subduction-accretion processes of the southern Altaids. American Journal of Science 309, 221−270.

Xiao, X.C., Tang, Y.Q., Feng, Y.M., Zhu, B.Q., Li, J.Y., Zhao, M., 1992. The Tectonic Structure of the Northern Xinjiang and its Adjacent Regions. Geological Publishing House, Beijing, 169 pp (in Chinese).

Xu, J.F., Castillo, P.R., Chen, F.R., Niu, H.C., Yu, X.Y., Zhen, Z.P., 2003. Geochemistry of late Paleozoic mafic igneous rocks from the Kuerti area, Xinjiang, northwest China: implications for backarc mantle evolution. Chemical Geology 193, 137−154.

Xu, J.F., Chen, F.R., Yu, X.Y., Niu, H.C., Zheng, Z.P., 2001. Kuerti ophiolite in Altay area of North Xinjiang: magmatism of an ancient back-arc basin. Acta Petrologica et Mineralogica 20 (3), 344−352 (in Chinese with English abstract).

Yakubchuk, A., 2004. Architecture and mineral deposit settings of the Altaid orogenic collage: a revised model. Journal of Asian Earth Sciences 23, 761−779.

Yin, A., Nie, S., 1996. A Phanerozoic palinspastic reconstruction of China and its neighboring regions. In: Yin, A., Harrison, T.M. (Eds.), The Tectonic Evolution of Asia. Cambridge University Press, Cambridge, pp. 442−485.

Yu, X.Y., Niu, H.C., Xu, J., Chen, F.R., Zheng, Z.P., 2000. On the Fluid System of the Paleozoic Volcano-sedimentary Basins and Associated Mineralization. Chinese National 305 Project, Urumqi. pp. 181 (in Chinese).

Zhang, C., 1981. Some geological characters of the ophiolite of Xinjiang. Geological Review 7 (4), 307−314 (in Chinese with English abstract).

Zhang, H.X., Niu, H.C., Kentaro, T., Yu, X.Y., Soto, H., Ito, J., 2003a. Zircon SHRIMP U-Pb dating on plagiogranite from Kuerti ophiolite in Altay, North Xinjiang. Chinese Science Bulletin 48, 2231−2235.

Zhang, H.X., Shen, X.M., Ma, L., Niu, H.C., Yu, X.Y., 2008a. Geochronology of the Fuyun adakite, north Xinjiang and its constraint to initiation of the Paleo-AsianOcean subduction. Acta Petrologica Sinica 24 (5), 1054−1058 (in Chinese with English abstract).

Zhang, Q., Wang, C.Y., Liu, D., Jian, P., Qian, Q., Zhou, G., Robinson, P.T., 2008b. Brief review of ophiolites in China. Journal of Asian Earth Sciences 32, 308−324.

Zhang, Q., Wang, Y., Zhou, G.Q., Qian, Q., Robinson, P.T., 2003b. Ophiolites in China, their distribution, ages and tectonic settings. In: Dilek, Y., Robinson, P.T. (Eds.), Ophiolites in Earth History. Geological Society, London, Special Publication 218, pp. 541−566.

Zhang, Q., Zhou, G.Q., 2001. Ophiolites of China. Science Press, Beijing, 182 pp (in Chinese with English abstract).

Zhang, X.B., Sui, J.X., Li, Z.C., Liu, W., Yang, X.Y., Liu, S.S., 1996. Tectonic Evolution of the Erqis Belt and its Mineral Deposit Series. Science Press, Beijing, 205 pp (in Chinese).

Zhang, Z.C., Zhou, G., Kusky, T.M., Yan, S.H., Chen, B.L., Zhao, L., 2009. Late Paleozoic volcanic record of the Eastern Junggar terrane, Xinjiang, Northwestern China: major and trace element characteristics, Sr-Nd isotopic systematics and implications for tectonic evolution. Gondwana Research 16, 201−215.

Zonenshain, L.P., Kuzmin, M.I., Natapov, L.M., 1990. Geology of the USSR: A Plate Tectonic Synthesis. In: Geodynamic Series 21. American Geophysical Union, Washington, D.C., 242 pp.